Desalination and Water Treatment
www.deswater.com
doi: 10.1080/19443994.2014.996773

57 (2016) 5108–5118
March

Taylor & Francis
Taylor & Francis Group

Adsorption of dibenzothiophene sulfone from fuel using chitosan-coated bentonite (CCB) as biosorbent

Ming-Chun Lu[a], Luisa Cyd Charisse Biel[b], Meng-Wei Wan[a,*], Rizalinda de Leon[c], Susan Arco[d], Cybelle M. Futalan[e]

[a]*Department of Environmental Resources Management, Chia-Nan University of Pharmacy and Science, Tainan 71710, Taiwan, emails: mmclu@mail.chna.edu.tw (M.-C. Lu), peterwan@mail.cnu.edu.tw (M.-W. Wan)*
[b]*Environmental Engineering Graduate Program, University of Philippines-Diliman, Quezon City 1800, Philippines, email: luisa.biel@gmail.com*
[c]*Department of Chemical Engineering, University of Philippines-Diliman, Quezon City 1800, Philippines, email: rldeleon@up.edu.ph*
[d]*Institute of Chemistry, University of Philippines-Diliman, Quezon City 1800, Philippines, email: wann612@yahoo.com*
[e]*Operations Department, Frontier Oil Corporation, Makati City 1229, Philippines, email: cmfutalan@gmail.com*

Received 11 May 2014; Accepted 28 November 2014

ABSTRACT

Removal of dibenzothiophene sulfone (DBTS) from fuel onto chitosan-coated bentonite (CCB) was investigated using a fixed-bed column system. The experiments were carried out as a function of flow rate, particle size, and initial feed of DBTS concentration. The bed adsorption capacities were found to increase with the decreasing flow rate and particle size. Maximum bed adsorption capacities for the various flow rates were found to be 4.30, 3.09, and 2.44 mg DBTS/g CCB at 1, 5, and 10 mL/min, respectively. When the initial DBTS concentration was increased from 500 to 1,000 mg/L, the corresponding adsorption bed capacity appears to increase from 4.31 to 5.55 mg/g. Spectra studies showed possible involvement of hydroxyl groups in the biosorption. The Thomas model was used to predict the breakthrough curves under varying experimental conditions. Results indicate a good agreement between the experimental data and predicted breakthrough curves generated by the Thomas model.

Keywords: Chitosan; Bentonite; Dibenzothiophene; Sulfone; Thomas Model

1. Introduction

Presence of sulfur in diesel fuel is of great concern because combustion of sulfur-laden diesel fuel leads to the production of sulfur dioxide and sulfate particulate matter. The accumulation of sulfur dioxide and nitrogen oxide in the atmosphere results in the formation of acid rain, while sulfate particulate matter can cause respiratory problems [1]. Thus, stringent regulations on the amount of sulfur in diesel fuel were implemented worldwide. In the regulation issued by the United States Environmental Protection Agency, the sulfur content in diesel fuel was reduced to ultra-low sulfur diesel (ULSD) (<15 ppm) in 2010 for health and environmental protection [2].

*Corresponding author.

Currently, a combined process of ultrasound-assisted oxidation and adsorption has demonstrated favorable results in achieving ULSD. The principle behind these techniques involves the conversion of refractory sulfur and other sulfur containing compounds into their corresponding sulfoxides and sulfones using an oxidant [3,4]. These more polar products can be easily removed by solid adsorption at low temperature and ambient pressure. The adsorption of the oxidized sulfur compounds such as dibenzothiophene sulfone (DBTS) onto solid adsorbents allows for their removal from fuel without the addition of chemicals [5].

To date, the adsorbents that have been employed for the removal of DBTS were activated carbon and alumina, specifically acidic alumina. In the study conducted by Etemadi and Yen [5], acidic alumina exhibits good adsorption capacity for oxidized refractory sulfur compound as compared to activated carbon. However, the use of acidic alumina as adsorbent is quite expensive. These constraints have caused the search for alternative technologies for the adsorption of the oxidized sulfur compounds to cost-effective environmentally acceptable levels.

In recent years, the use of polymeric adsorbents for the removal of pollutants in wastewater had been extensively used due to their adsorption-regeneration properties and mechanical strength. An example of this is chitosan, a polysaccharide produced by alkaline deacetylation of chitin that is primarily found in shells of shrimps [6,7]. Chitosan has been proved as a useful material for removing inorganic and organic substances from wastewater due to the presence of primary, secondary hydroxyl groups, and highly reactive amino groups. Furthermore, chitosan has the advantage of being nontoxic and biodegradable [8]. However, chitosan alone is not an ideal bioadsorbent due to several disadvantages that include low-surface area, low specific gravity, softness and weak mechanical properties [9,10]. Moreover, chitosan easily dissolves in acidic solutions and at the same time tends to form a hydrogel in aqueous media. This results in the inaccessibility of its binding sites. Therefore, to improve its strength for practical applications chitosan is modified either chemically or physically [11].

Several investigators have attempted to modify the chitosan in order to facilitate mass transfer and expose the active binding sites for the enhancement of its adsorption capacity. These include crosslinking or chitosan derivative based on carboxymethyl and hydroxamic acid, and coating bentonite with chitosan [9]. But the former is rather costly and/or has complicated preparative methods as compared to the latter that is simple to prepare. In addition, according to various studies, the latter method greatly reduces the amount of chitosan used during synthesis in order to produce the needed composite adsorbent material with improved mechanical and chemical stability, and as a result lowers the production cost [12,13].

The effectiveness of utilizing chitosan coated on bentonite for the removal of heavy metals in batch studies and column studies has been demonstrated in several studies [12,14,15]. Their experimental results showed that chitosan coated on bentonite was very effective in the removal of copper (II) [12,14,15], lead (II) [15], and nickel (II) [15] from aqueous solutions. Previous researches utilized chitosan crosslinked with glutaric dialdehyde and glutarahdehyde in removing DBTS from acetonitrile solution, and showed the effectiveness of chitosan in removing oxidized sulfur compounds from fuels [16,17]. Moreover, Lu et al. reported on the kinetics and isotherm of the removal of DBTS using chitosan-coated bentonite (CCB) [18]. However, there are no fixed-bed studies on chitosan and its derivatives as an adsorbent utilized for clean fuel production.

Thus, in this work, a composite chitosan bioadsorbent was investigated in the removal of oxidized sulfur compound from model diesel fuel in a fixed-bed column system. The CCB is prepared by coating chitosan, a glucosamine biopolymer, over bentonite, a type of clay material that has a high specific surface area and is mechanically and chemically stable and formed into beads. It is expected that more active sites of chitosan will be available, thus enhancing its adsorption capacity. The CCB beads are characterized before and after adsorption of the oxidized sulfur compounds by Fourier transform infrared (FTIR) spectroscopy, thermal gravimetric analysis (TGA), and scanning electron microscopy (SEM). The effect of influent concentration, particle, flow rate on the column performance, and the shape of the breakthrough curves will be evaluated. Kinetic column model namely Thomas model will be applied to describe the dynamic performance of the adsorption process and assist in predicting the breakthrough curves.

2. Materials and experimental methods

2.1. Materials

All reagents used were of analytical grade and were utilized as received without further purification. DBTS with quoted purities of 0.98 mass fractions was obtained from Alfa Aesar. These compounds are representative of the sulfur compounds found in diesel fuel. Toluene (as solvent), NaOH pellets, and hydrochloric acid (HCl) fuming 37% were purchased from

Merck Germany with quoted purities of 0.99 mass fractions. Low-molecular weight powdered chitosan (MW 340.3322 g/mole extracted from crab shells) with 75–85% degree of deacetylation and viscosity of 20 cP was procured from Sigma-Aldrich. The bentonite, as substrate, was obtained from First Chemical. Water used for the preparation of solutions and cleaning the adsorbents was generated in the laboratory by double distilling the deionized water in a quartz distillation unit.

2.1.1. Adsorbate

The initial concentrations of the stock solution for the oxidized sulfur compound (DBTS) were regulated to approximately 500, 750, and 1,000 ppm. This was prepared by mixing appropriate amount of DBTS in toluene. The amount of the polar sulfur compound in the fuel was analyzed using the Gas Chromatography (GC)–Sulfur Chemiluminescence Detector (SCD).

2.1.2. Synthesis of adsorbent

In the synthesis of the adsorbent, about 5 g chitosan was mixed with 300 mL of 5% (v/v) HCl and the mixture was stirred for 2 h at the rated speed of 300 rpm. Then, 100 g of bentonite was slowly added into the solution under continuous stirring and the mixture was stirred for another 3 h. Bentonite, which is composed mainly of montmorillonite clay, was used as substrate for the preparation of beads. Precipitation of the chitosan on the bentonite was carried out by the dropwise addition of 1 N NaOH. The addition of NaOH solution was done until neutralization occurs and synthesized adsorbent was washed several times with deionized water. The adsorbent was then dried in the oven at 65°C for 24 h and sieved to the desired particle size range of 0.1–1.5 mm.

2.2. Experimental methods

A schematic diagram of the fixed-bed column system utilized in this study is shown in Fig. 1. Dynamic flow adsorption studies were carried out in a column made of borosilicate glass from IWAKI glass code 7740 with a 1.2 cm internal diameter and 55 cm in height. The column was first filled with glass beads to serve as support material. Then, 10 g of CCB was added by tapping so that the column was filled without gaps followed by a glass mesh to control the flow of the inlet solution. The adsorbent was washed thoroughly with toluene prior to use to ensure all the pore spaces were filled.

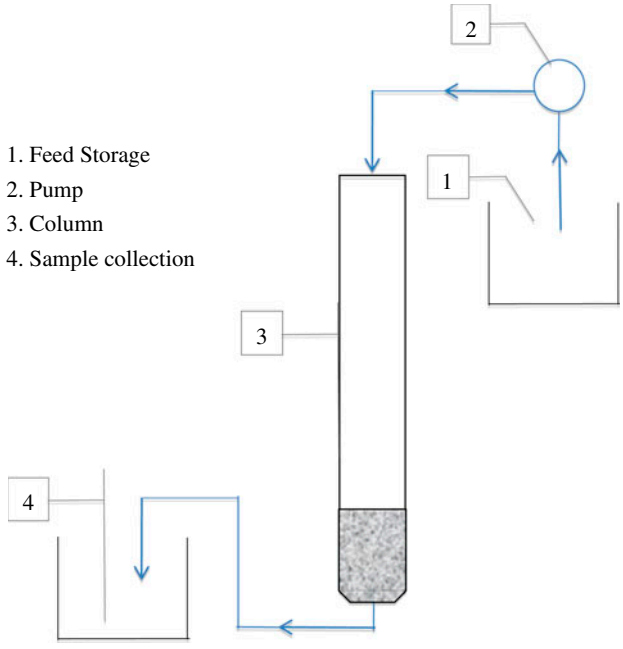

Fig. 1. Experimental system for fixed-bed column.

In a typical experiment, the influent solution was fed from the top of the column using a peristaltic pump (Masterflex CZ 77120-70) at room temperature. Samples were collected at the bottom of the column at regular time intervals. Column experiments were operated in a down flow manner. To study the effect of parameters such as flow rate (1, 5, and 10 mL/min), particle size (0.1–0.5, 0.5–1.0, and 1.0–1.5 mm), and initial concentration of DBTS (500, 750, and 1,000 ppm), the experiments were conducted by varying one parameter at a time while keeping all other parameters constant. The complete cycle of operation of each column experiment includes two steps: obtaining constant solution flow and adsorption of solute (DBTS) until column exhaustion occurs. Effluent solution was collected at predetermined time intervals and preserved for analysis. The solutions were diluted appropriately prior to analysis. All experiments were carried out at room temperature. Breakthrough curves were obtained by plotting the volume of the solution that passed through the column against ratio of the column effluent concentration to the initial concentration, C_t/C_0.

2.3. Analytical methods and instrumentation

To determine the amount of sulfur in the oxidized solution, the Agilent Technologies 7890A GC System equipped with a fused-silica capillary HP-5 ms column (30 m) having a thickness of 0.25 mm film (J & W

Scientific, Folsom, CA, USA) was employed. The GC was connected to a SCD for higher selectivity and sensitivity towards ultra-low sulfur concentration. The GC temperature was initially set to 100°C for 3 min and ramped up to 300°C at increasing rate of 20°C/min.

SEM was performed using a Philips-FEI XL30 ESEM-TMP (Philips Electronics Co., Eindhoven) to determine the morphology of the adsorbent. Images of various materials were obtained at an operating voltage of 10 kV. Moreover, TGA was performed on freeze-dried bentonite, chitosan, and CCB samples using Rigaku Thermo Plus TG 8120 in the temperature range of 30–800°C at a heating rate of 10°C/min. The FTIR spectra of the adsorbent materials were recorded utilizing a Perkin Elmer 1800 model IR spectrophotometer with operating frequencies that ranges between 400 and 4,000 cm^{-1}.

2.4. Analysis of column data

In determining the operation and response of an adsorption column, there are two important characteristics that should be considered. These include the time at breakthrough and the shape of the breakthrough curve. The importance of a breakthrough curve illustrates the uptake of the DBTS in a fixed-bed system. This is usually expressed in terms of normalized concentration or the ratio of effluent (desulfurized feed containing DBTS after adsorption) concentration to influent (desulfurized feed containing DBTS before adsorption) concentration (C_t/C_0) as a function of time or volume of effluent for a given bed height. The treated effluent volume (V_{te}) is given by Eq. 1:

$$V_{te} = Qt_{ex} \tag{1}$$

where Q *is* the volumetric flow rate (mL/min) and t_{ex} is the time at exhaustion (min), respectively. The breakthrough and exhaustion points refer to when the effluent reaches 10 and 90% of the influent concentration, respectively.

For the total DBTS adsorbed (q_{total}) in the column, this can be determined through the area under the breakthrough curve (A). The area can be calculated by integrating the adsorbed DBTS concentration (C_{ad} = inlet DBTS concentration (C_0)−outlet DBTS concentration (C_t)) vs. t (min) plot. Total DBTS adsorbed quantity (q_{total}; mg) in the column is expressed in Eq. 2:

$$q_{total} = \frac{QA}{1{,}000} = \frac{Q}{1{,}000}\int_{t=0}^{t=t_{total}} C_{ad}\mathrm{d}t \tag{2}$$

The total amount of DBTS sent to column (m_{total}) is calculated from Eq. 3:

$$m_{total} = \frac{C_0 Q t_{total}}{1{,}000} \tag{3}$$

Total removal (Y) is shown and calculated from Eq. 4:

$$Y\ (\%) = \frac{q_{total}}{m_{total}} \times 100 \tag{4}$$

The equilibrium uptake (q_e) or the maximum capacity of the column, which is the weight of adsorbate adsorbed per unit dry weight of adsorbent (mg/g) in the column, is calculated as follows (Eq. (5)):

$$q_e = \frac{q_{total}}{X} \tag{5}$$

where X is the total dry weight of adsorbent in the column (g).

2.5. Mathematical model

The ability to predict the concentration–time profile or breakthrough curve for the effluent is the determining point in the effective design of a column system. There are a number of mathematical models that can be employed to describe a fixed-bed column system. One of the simple and most widely used models is the Thomas or reaction model. The model assumes the Langmuir kinetics of adsorption–desorption and no axial dispersion in the column adsorption. The reason for this is derived from the adsorption that the rate-driving force obeys second-order reversible reaction kinetics. Thomas' solution also assumes a constant separation factor but it is applicable to either favorable or unfavorable isotherms [19]. The Thomas model given by the Eq. (6) is as follows [20,21]:

$$\frac{C_t}{C_0} = \frac{1}{1 + \exp\left(\left(\frac{k_{TH}}{Q}\right)(Q_e X - C_0 V_{te})\right)} \tag{6}$$

where k_{TH} is the Thomas rate constant (mL/min mg); Q_e is the maximum solid-phase concentration of solute (mg/g). X is the amount of adsorbent in the column (g); and V_{te} is the effluent volume (L); Q is the flow rate (mL/min).

The linearized form of the Thomas model is shown in Eq. 7:

$$\ln\left(\frac{C_0}{C_t}-1\right)=\frac{k_{TH}Q_eX}{Q}-\frac{k_{TH}C_0V_{te}}{Q} \quad (7)$$

where a plot of ln $[(C_t/C_0)-1]$ against C_0 at given conditions will determine the kinetic coefficient k_{TH} and the adsorption capacity of the bed Q_e.

3. Results and discussion

3.1. Scanning electron microscopic studies

The SEM micrographs of pure chitosan and bentonite are shown in Fig. 2(a) and (b), respectively. Fig. 2(a) illustrates the surface texture of the chitosan that shows a continuous, smooth, and non-porous surface [22]. Fig. 2(b) illustrates the morphology of the bentonite, where coarser and more porous surface area was observed.

Fig. 2(c) and (d) represents the SEM micrograph of the adsorbent before and after adsorption, respectively. In Fig. 2(c), the surface morphology of CCB exhibits a structure similar to bentonite but with lesser pores. The coating of chitosan onto bentonite surface has lessened the porosity of the bentonite particles. Comparing Fig. 2(c) and (d), there were no significant changes observed.

3.2. TGA studies

To confirm the successful coating of chitosan onto bentonite, the results from TGA are presented in Fig. 3. The chitosan has two decomposition sites: the first one is at 50–120°C that is attributed to loss of

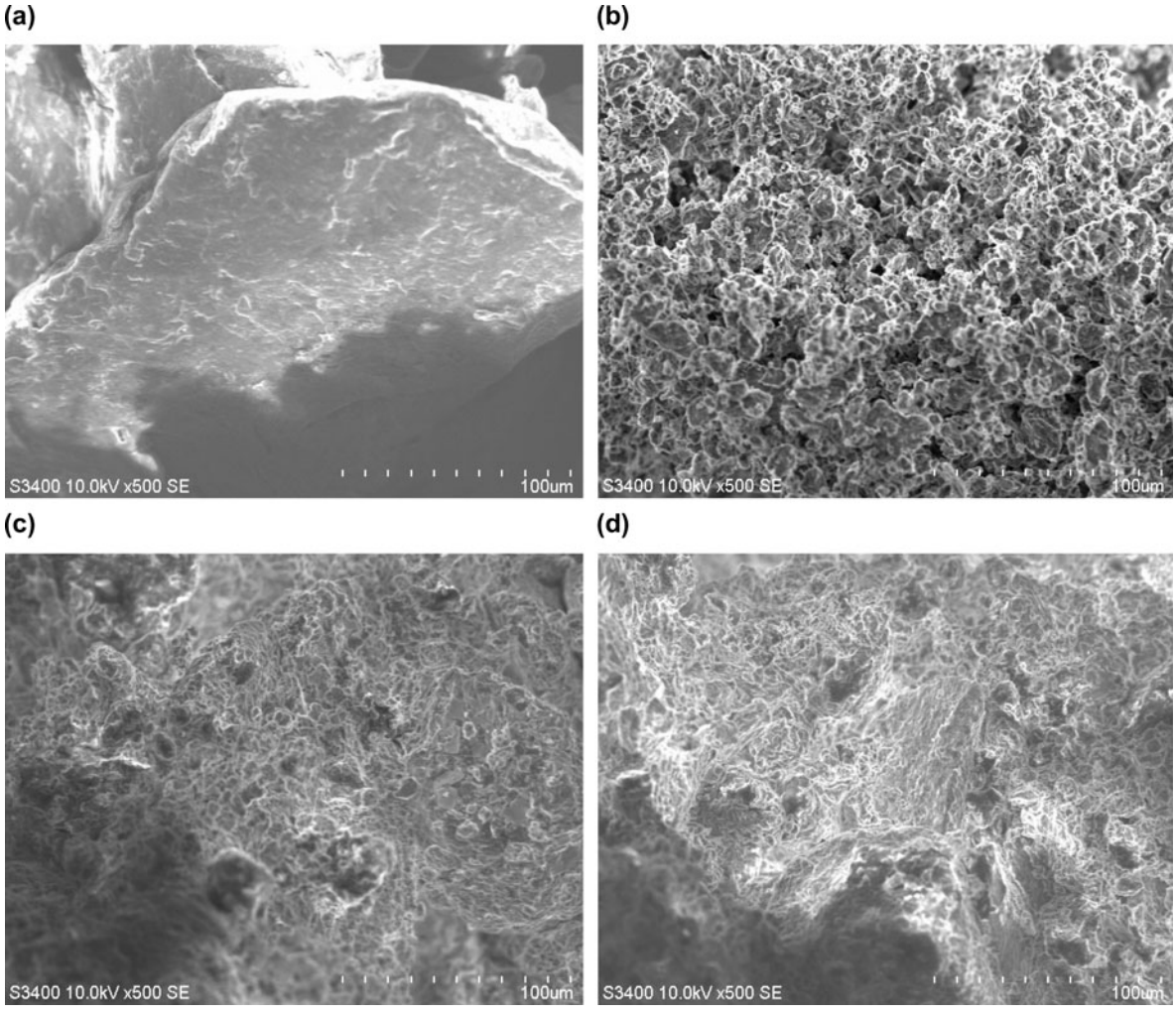

Fig. 2. SEM images of (a) chitosan, (b) bentonite, (c) synthesized CCB before adsorption, and (d) synthesized CCB after adsorption with oxidized sulfur compound solution.

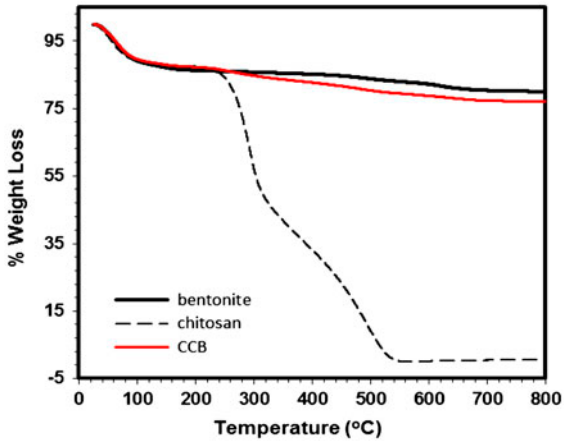

Fig. 3. TGA of CCB.

physically adsorbed water [23]. The second decomposition occurred at 240°C, which was due to the degradation of the chitosan molecular structure. It was then completely burnt out at 600°C. The carrier, bentonite, has two sites that illustrates the weight loss at 90°C (evaporation of adsorbed water) and 450–600°C (loss of hydroxyl structural group) [24]. The thermogram of CCB which shows similar decomposition stages to that of bentonite has a relatively larger weight loss.

3.3. FTIR studies

The FTIR spectra of CCB before and after adsorptions were investigated to determine the interaction between DBTS and functional groups of CCB (Fig. 4). In Fig. 4(a), abroad absorption peak at 3,622 and 3,376 cm^{-1} is shown that corresponds to the stretching vibrations of bonded –OH groups [22]. The peaks at 1,637 and 1,567 cm^{-1} represents the vibrations of carbonyl bonds (C=O group) of amide groups and vibrations of amine group ($–NH_2$), respectively [25]. The bands observed at about 1,012 cm^{-1} could be assigned to vibration stretching of CO group [26]. The peaks observed at 793 cm^{-1} could be assigned to $R–NH_2$ stretching [25].

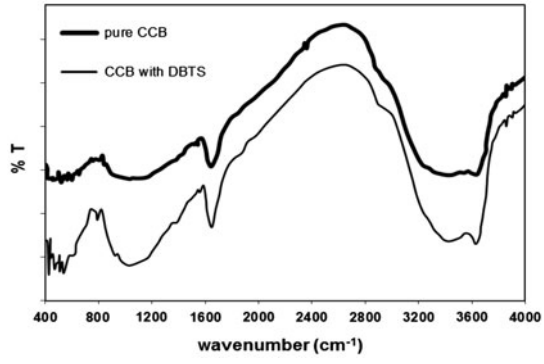

Fig. 4. FTIR spectral of CCB (a) before and (b) after adsorption of DBTS.

There are several peaks observed to shift and/or broadened in the FTIR spectra of CCB before and after adsorption, which indicates that functional groups present on CCB was involved in the interaction with DBTS. From Table 1, a significant shift at 3,622 cm^{-1} was observed, which implies that the bonded –OH groups of CCB were especially involved as potential active binding sites in the adsorption of the DBTS.

3.4. Effect of flow rate

The influence of flow rate on the biosorption of DBTS by CCB was investigated by keeping the initial DBTS concentration of 500 ppm and particle size of 1 mm constant and varying the flow rate from 1 to 10 mL/min.

As illustrated in Fig. 5, a low flow rate of 1 mL/min causes rapid adsorption of DBTS. When the flow rate was increased, the breakthrough curve becomes steeper with which an earlier breakthrough and exhaustion time were observed. Furthermore, the highest DBTS removal of 56.72% and highest bed adsorption capacity at exhaustion was obtained at 4.28 mg sulfur/g adsorbent at low flow rate (1 mL/min). In comparison to only 40.66% removal and 2.41 mg DBTS/g adsorbent adsorption capacity were attained at high low rates (10 mL/min).

Initially, an increase in flow rate from 1 to 10 mL/min decreases the volume of effluent treated from 150.00 to 130.00 mL and removal efficiency of DBTS. The probable reason behind this is a high flow rate that results in shorter residence time in the column. If the saturation time of the solute in the fixed-bed column was not long enough for the adsorption equilibrium to be reached at high flow rate (10 mL/min), DBTS solution leaves the adsorption column before equilibrium occurs. As the adsorption rate was controlled by intraparticulate diffusion, an early breakthrough occurs leading to a low bed adsorption capacity [27]. Moreover, an increase in the flow rate reduces the volume treated efficiently until breakthrough point and therefore decreases the service time of the bed. Thus, the contact time of DBTS with CCB was very short at higher flow rate, causing a reduction in removal efficiency. The study of Ghorai and Pant showed similar results, where the removal efficiency of fluoride with activated alumina decreases as the flow rate increases [28].

Table 1
FTIR spectral characteristics of CCB before and after adsorption for DBTS

IR peak	Frequency (cm^{-1})			Assignment
	Before adsorption	After adsorption (DBTS)	Differences	
1	3,622	3,622	0	Bonded –OH groups
2	3,376	3,385	+9	Bonded –OH groups
3	1,567	1,565	−2	Vibrations of amine groups ($–NH_2$)
4	1,637	1,635	–2	C=O stretching
5	1,012	1,007	–5	CO stretching
6	793	792	–1	R–NH2 stretching

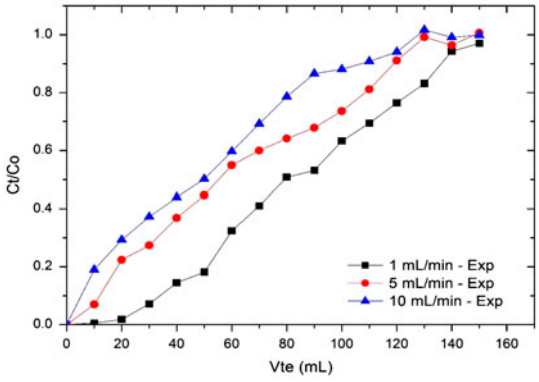

Fig. 5. Breakthrough curve for DBTS adsorption onto CCB under different flow rates.

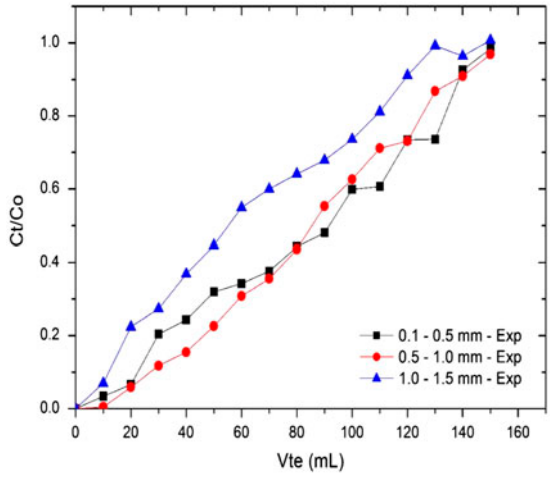

Fig. 6. Breakthrough curve for DBTS adsorption onto CCB under different particle sizes.

Table 2
Effect of varying flow rate, particle size, and initial concentration on DBTS adsorption using CCB

	Parameters			
	q_{total} (mg)	m_{total} (g)	Total removal (%)	q_e (mg/g)
Flow rate[a]				
1 mL/min	42.82	75.49	56.72	4.28
5 mL/min	30.68	64.71	47.41	3.07
10 mL/min	24.12	59.32	40.66	2.41
Particle size[b]				
0.1–0.5 mm	43.17	70.10	61.58	4.32
0.5–1.0 mm	41.38	67.40	61.39	4.14
1.0–1.5 mm	30.68	64.71	47.41	3.07
Initial concentration[c]				
500 ppm	42.82	75.49	56.72	4.28
750 ppm	53.23	98.09	54.27	5.32
1,000 ppm	54.81	105.71	51.85	5.48

[a]Particle size = 1–1.5 mm; initial DBTS concentration = 500 ppm.
[b]Flow rate = 5 mL/min; initial DBTS concentration = 500 ppm.
[c]Particle size = 1–1.5 mm; flow rate = 1 mL/min.

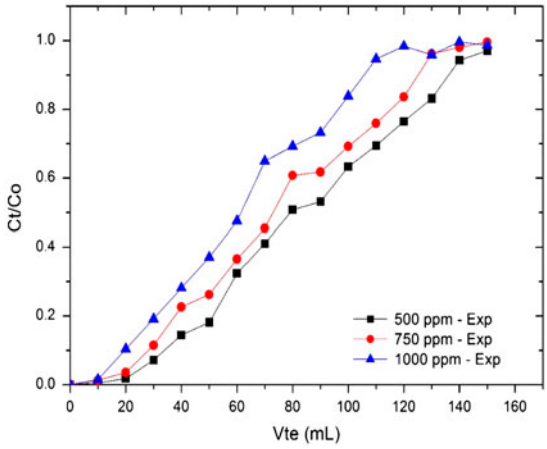

Fig. 7. Breakthrough curve for DBTS adsorption onto CCB at different initial concentrations.

3.5. Effect of particle size

DBTS adsorption in fixed-bed column system was tested under varying particle sizes (0.1–1.5 mm) where influent concentration of 500 ppm and flow rate of 5 mL/min was kept constant. In Fig. 6, the breakthrough curves obtained at different particle sizes, 0.10–0.50, 0.50–1.00, and 1.00–1.50 mm, were illustrated. When the particle size was increased from 0.1 to 1 mm, an increase in the slope from the point of breakthrough up to point of exhaustion was observed. The reason for this is that smaller particles will have a shorter diffusion path, thus allowing the adsorbate to penetrate deeper into the adsorbent particle more quickly. This phenomenon results in a higher rate of adsorption for 0.1 mm particle size. In addition, smaller particles have larger total external surface area per unit volume that permits sufficient amount of DBTS to be adsorbed onto CCB.

In Table 2, a decrease in the particle size range from 1.00–1.50 to 0.10–0.5 mm results in a significant increase in DBTS adsorbed, total removal, and adsorption capacity. The increase in treated capacity as the particle size decreases is probably due to a higher overall rate of diffusion resulting from the availability of greater interfacial area and adsorbent dosage [29]. It is expected that the smaller diameter will have a higher adsorption capacity because of greater outer surface area per unit volume. However, it has been reported that small particle sizes are to be avoided as it results in high-flow resistance of the column [30].

3.6. Effect of initial concentration

Initial DBTS concentrations of 500, 750, and 1,000 mg/L were studied while the flow rate of 1 mL/min and particle size of 1 mm were kept constant. In contrast to the previous parameters, the column performed well at highest concentration in terms of adsorption capacity. An increase of the initial concentration significantly affects the shape of breakthrough curve (Fig. 7). The DBTS breakthrough curves was observed to become steeper at 1,000 ppm.

Higher initial DBTS concentration results to a faster breakthrough as expected. The driving force for biosorption was the concentration difference between DBTS concentration on adsorbent and in solution [20]. Thus, a higher driving force caused by high DBTS concentration resulted in better column performance.

Table 3
Column parameters at different flow rates, particle sizes, and initial concentrations obtained through Thomas model

	Correlation coefficient, R^2	k_{TH} (mL/min mg)	Q_e (mg/g)
Flow rate[a]			
1 mL/min	0.945	0.090	4.700
5 mL/min	0.912	0.386	3.520
10 mL/min	0.937	0.890	2.550
Particle size[b]			
0.1–0.5 mm	0.918	0.430	4.690
0.5–1.0 mm	0.943	0.360	4.390
1.0–1.5 mm	0.912	0.386	3.520
Initial concentration[c]			
500 ppm	0.945	0.090	4.700
750 ppm	0.947	0.075	5.650
1,000 ppm	0.946	0.060	6.070

[a]Particle size = 1–1.5 mm; initial DBTS concentration = 500 ppm.
[b]Flow rate = 5 mL/min; initial DBTS concentration = 500 ppm.
[c]Particle size = 1–1.5 mm; flow rate = 1 mL/min.

In Table 2, the initial DBTS concentration was increased from 500 to 1,000 ppm causes a corresponding increase in adsorption bed capacity from 4.28 to 5.48 mg/g. A decrease in influent concentration causes the slow transport of DBTS due to the decreased diffusion coefficient and decreased mass transfer driving force [31]. At 1,000 ppm, the adsorbent bed was observed to be saturated quickly that caused decrease in total DBTS removal and earlier breakthrough and exhaustion time. Moreover, the maximum removal obtained for 500, 750, and 1,000 ppm were 56.72, 54.27, and 51.85% respectively.

3.7. Breakthrough curve model

In Table 3, the correlation coefficient values and Thomas constants (k_{TH} and Qe) for DBTS are shown. The obtained values for correlation coefficient ranges from 0.912 to 0.945.

In Table 3, the k_{TH} value slightly decreases with increasing initial concentration due to the increase in driving force that facilitates the mass transfer in solution. In addition, the adsorption bed capacity values fairly increase as the inlet DBTS concentration increases. These results were in correlation with those observed from the experimental breakthrough curves. The predicted Q_e values for DBTS were observed to decrease with increasing flow rate. The k_{TH} values, on the other hand, increase with increasing flow rate due to decrease in the mass transport resistance. Values of the predicted Q_e obtained from the Thomas model were 4.70, 3.52, and 2.55 mg/g for 1, 5 and 10 mL/min, respectively. The sorption data showed that the predicted Q_e value decreases with increasing particle size of CCB. However, increasing the particle size does not affect k_{TH} value for DBTS.

The plot between experimental data and theoretical points under all experimental conditions is illustrated in Fig. 8. The results indicate that there is a good agreement between the experimental and the predicted bed capacities at all tested experimental parameters.

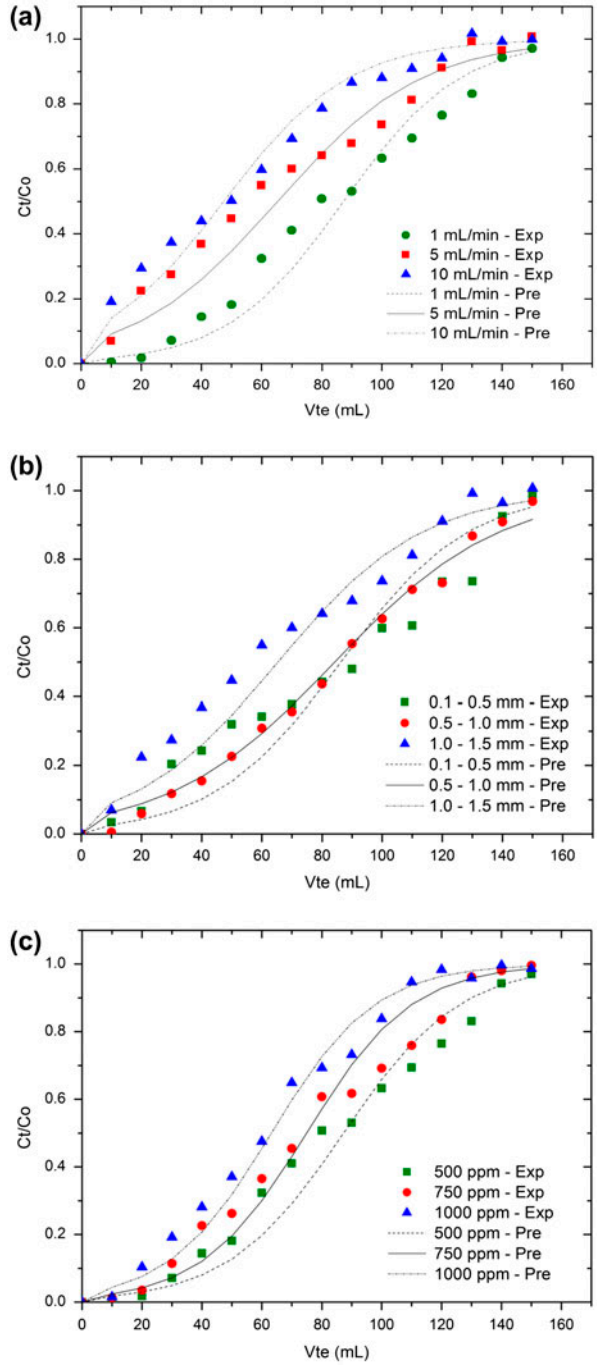

Fig. 8. Experimental and predicted breakthrough curve for DBTS under different (a) flow rates (b) particle sizes, and (c) initial concentrations.

3.8. Mechanism of adsorption

The adsorption of DBTS onto the CCB was investigated in order to get some insight into the nature of the mechanism of adsorbent–adsorbate interaction. Due to the polar nature of DBTS, it can be easily adsorbed compared to dibenzothiophene. Consequently, FTIR technique is utilized in order to determine the interaction between an adsorbate and the active groups on the surface of adsorbent [32]. Based on FTIR analysis, hydroxyl was the main functional group involved in DBTS adsorption onto the adsorbent. The oxygen atom present in the oxidized sulphur compound makes a bond with the hydrogen molecules of the hydroxyl group.

Moreover, isotherm studies conducted by Lu et al. illustrate that DBTS follows the Langmuir isotherm which indicates that DBTS would only bind to one type of functional group present in CCB [18]. This further validates the results of FTIR analysis, where hydroxyl (–OH) groups are the functional groups in CCB that adsorb DBTS.

The adsorption kinetics follows the pseudo-second-order rate model for DBTS involving valency forces through sharing or exchange of electrons between sorbent and sorbate [33]. This suggests the main mechanism of adsorption was chemisorption that involves the formation of strong chemical bonds between adsorbent and DBTS.

4. Conclusion

In this study, the removal of DBTS from fuel using CCB was investigated. The FTIR spectra showed that bonded –OH groups serve as binding sites for the adsorption of DBTS onto CCB. Result showed that flow rate, influent concentration, and particle size affects the shape of the breakthrough curve. Maximum DBTS adsorption capacity of 4.32 DBTS/g CCB was achieved using 0.1–0.5 mm (particle size) and 5 mL/min (flow rate). The Thomas model adequately described the adsorption of DBTS onto CCB by fixed-bed column system. Thus, this effective biosorbent could be applied to novel desulfurization technology (UAOD process) to obtain the ultra-low sulfur oil.

Acknowledgments

The authors would like to gratefully acknowledge the National Science Council of Taiwan (Contract No. NSC 101-2221-E-041-010-MY3) and the Engineering Research and Development for Technology for financially supporting this research.

References

[1] T.O. Sachdeva, K.K. Pant, Deep desulfurization of diesel via peroxide oxidation using phosphotungstic acid as phase transfer catalyst, Fuel Process. Technol. 91 (2010) 1133–1138.
[2] H. Lü, C. Deng, W. Ren, X. Yang, Oxidative desulfurization of model diesel using [(C4H9)4N]6Mo7O24 as a catalyst in ionic liquids, Fuel Process. Technol. 119 (19) (2014) 87–91.
[3] H. Mei, B.W. Mei, T.F. Yen, A new method for obtaining ultra-low sulfur diesel fuel via ultrasound assisted oxidative desulfurization, Fuel 82 (2003) 405–414.
[4] M.W. Wan, T.F. Yen, Enhance efficiency of tetraoctylammonium fluoride applied to ultrasound-assisted oxidative desulfurization (UAOD) process, Appl. Catal., A 319 (2007) 237–245.
[5] O. Etemadi, T.F. Yen, Aspects of selective adsorption among oxidized sulfur compounds in fossil fuels, Energy Fuels 21 (2007) 1622–1627.
[6] P.K. Dutta, J. Dutta, V.S. Tripathi, Chitin and chitosan: Chemistry, properties and applications, J. Sci. Ind. Res. 63 (2004) 20–31.
[7] M. Rinaudo, Chitin and chitosan: Properties and applications, Prog. Polym. Sci. 31 (2006) 603–632.
[8] G. Crini, Non-conventional low-cost adsorbents for dye removal: A review, Bioresour. Technol. 97 (2006) 1061–1085.
[9] M.Y. Chang, R.S. Juang, Adsorption of tannic acid, humic acid, and dyes from water using the composite of chitosan and activated clay, J. Colloid Interface Sci. 278 (2004) 18–25.
[10] S.R. Popuri, Y. Vijaya, V.M. Boddu, K. Abburi, Adsorptive removal of copper and nickel ions from water using chitosan coated PVC beads, Bioresour. Technol. 100 (2009) 194–199.
[11] E. Guibal, Interactions of metal ions with chitosan based sorbents: A review, Sep. Purif. Technol. 38 (2004) 43–74.
[12] C.M. Futalan, C.C. Kan, M.L. Dalida, C. Pascua, M.W. Wan, Fixed-bed column studies on the removal of copper using chitosan immobilized on bentonite, Carbohydr. Polym. 83 (2011) 697–704.
[13] L. Wang, A. Wang, Adsorption behaviors of Congo red on the N O-carboxymethyl-chitosan/montmorillonite nanocomposite, Chem. Eng. J. 143 (2008) 43–50.
[14] M.L.P. Dalida, A.F.P. Mariano, C.M. Futalan, C.C. Kan, W.C. Tsai, M.W. Wan, Adsorptive removal of Cu(II) from aqueous solutions using non-crosslinked and crosslinked chitosan-coated bentonite beads, Desalination 275 (2011) 154–159.
[15] C.M. Futalan, C.C. Kan, M.L. Dalida, K.J. Hsien, C. Pascua, M.W. Wan, Comparative and competitive adsorption of copper, lead and nickel using chitosan immobilized on bentonite, Carbohydr. Polym. 83 (2011) 528–536.
[16] J. Aburto, A. Mendez-Orozco, S. Borgne, Hydrogels as adsorbents of organosulphur compounds currently found in diesel, Chem. Eng. Process. 43 (2004) 1587–1595.
[17] J. Aburto, S. Le Borgne, Selective adsorption of dibenzothiophene sulfone by an imprinted and stimuli-responsive chitosan hydrogel, Macromolecules 37 (2004) 2938–2943.
[18] M.C. Lu, M.L. Agripa, M.W. Wan, M.L.P. Dalida, Removal of oxidized sulfur compounds using different types of activated carbon, aluminum oxide, and chitosan-coated bentonite, Desalin. Water Treat. 52 (2014) 873–879.
[19] P. Suksabye, P. Thiravetyan, W. Nakbanpote, Column study of chromium (VI) adsorption from electroplating industry by coconut coir pith, J. Hazard. Mater. 160 (2008) 56–62.
[20] Z. Aksu, F. Gönen, Biosorption of phenol by immobilized activated sludge in a continuous packed bed: Prediction of breakthrough curves, Process Biochem. 39 (2004) 599–613.
[21] Y. Fu, T. Viraraghavan, Column studies for biosorption of dyes from aqueous solutions on immobilised *Aspergillus niger* fungal biomass, Water SA 29 (2003) 465–472.

[22] A. Kamari, W.S. Ngah, Isotherm, kinetic, and thermodynamic studies of lead and copper uptake of H_2SO_4 modified chitosan, Colloids Surf., B 73 (2009) 257–266.
[23] T.S. Anirudhan, S. Rijith, Glutaraldehyde cross-linked epoxymated chitosan as an adsorbent for the removal and recovery for copper (II) from aqueous media, Colloids Surf., A 351 (2009) 52–59.
[24] G.V. Joshi, B.D. Kevadiya, H.A. Patel, H.C. Bajaj, R.V. Jasra, Montmorillonite as a drug delivery system: Intercalation and *in vitro* release of timolol maleate, Int. J. Pharm. 374 (2009) 53–57.
[25] C. Paluszkiewicz, E. Stodolak, M. Hasik, M. Blazewicz, FT-IR study of montmorillonite-chitosan nanocomposite materials, Spectrochim. Acta, Part A 79 (2011) 784–788.
[26] M.L. Duarte, M.C. Ferreira, M.R. Marvão, J. Rocha, An optimised method to determine the degree of acetylation of chitin and chitosan by FTIR spectroscopy, Int. J. Biol. Macromol. 31 (2002) 1–8.
[27] V.C. Taty-Costodes, H. Fauduet, C. Porte, Y.S. Ho, Removal of lead (II) ions from synthetic and real effluents using immobilized Pinus sylvestris sawdust: Adsorption on a fixed bed column, J. Hazard. Mater. 123 (2005) 135–144.
[28] S. Ghorai, K.K. Pant, Equilibrium, kinetics and breakthrough studies for adsorption of fluoride on activated alumina, Sep. Purif. Technol. 42 (2005) 265–271.
[29] M.J. Rivero, R. Ibáñez, M.I. Ortiz, Mathematical modelling of styrene drying by adsorption onto activated alumina, Chem. Eng. Sci. 57 (2002) 2589–2592.
[30] V.J. Inglezakis, H. Grigoropoulou, Effects of operating conditions on the removal of heavy metals by zeolite in fixed bed reactors, J. Hazard. Mater. 112 (2004) 37–43.
[31] T.V.N. Padmesh, K. Vijayaraghavan, G. Sekaran, M. Velan, Batch and column studies on biosorption of acid dyes on fresh water macro alga Azolla filiculoides, J. Hazard. Mater. 125 (2005) 121–129.
[32] P. Monash, G. Pugazhenthi, Adsorption of crystal violet dye from aqueous solution using mesoporous materials synthesized at room temperature, Adsorption 15 (2009) 390–405.
[33] Y. Sağ, Y. Aktay, Kinetic studies on sorption of Cr(VI) and Cu(II) ions by chitin, chitosan and Rhizopus arrhizus, Biochem. Eng. J. 12 (2002) 143–153.